Infrared Physics and Technology 98 (2019) 315–322

Contents lists available at ScienceDirect

Infrared Physics & Technology

journal homepage: www.elsevier.com/locate/infrared

Regular article

Liquid-type structure near-infrared light-emitting diodes based on PbSe quantum dots for acetylene gas detection

Xiaoxue Xing[a], Cheng Liu[a], Weiwei Shang[a], Hongwu Qin[a], Zhen Chen[b], Fucheng Cao[a,*]

[a] College of Electronic Information Engineering, Changchun University, Changchun 130012, China
[b] College of Information Engineering, Putian University, Putian 531100, China

ARTICLE INFO

Keywords:
Near-infrared
Acetylene gas detection
Liquid-type structure
PbSe QDs
NIR LEDs
Gas cell with ellipsoid reflector

ABSTRACT

Among near-infrared (NIR) absorption spectroscopy technique, an important limiting element is NIR light source, which will directly affect the performance of the gas detection system. In this paper, a liquid-type structure NIR light-emitting diodes (LEDs) based on PbSe quantum dots (QDs) is developed. Employing the NIR PbSe QDs LEDs, gas cell with ellipsoid reflector, photoelectric detector, STM32 main controller and signal processing module, a NIR gas differential detection system is designed to monitor acetylene gas. The experimental results show that the detection limit of the system is 10 ppm, and the maximum relative error of the system is less than ± 3%. A long-term measurement lasting for 20 h with the concentration of 200 ppm suggest that the system has good stability and reliability. Benefitting from the advantages of simple fabrication, narrow band, small size and easy tunability, the liquid-type NIR QDs-LEDs have great potential for gas analysis.

1. Introduction

As a colorless and flammable gas, acetylene (C_2H_2) is widely used in many industrial processes, such as metal cutting, metal welding, synthetic rubber and fiber, etc [1–3]. However, C_2H_2 will become dangerously explosive when its concentration reaches 7.73% in the air at ambient temperature and pressure [4,5]. In addition, C_2H_2 can also react with certain metals to generate explosive material easily. Therefore, it is extremely necessary and urgent to detect the concentration of C_2H_2 gas in industrial site.

NIR absorption spectroscopy is a well established technique used in gas sensing applications, providing high selectivity and sensitivity [6–9]. However, an important limiting element in NIR absorption method is the NIR light source. In the near-infrared, available sources include thermal radiation sources and semiconductor light-emitting diodes (LEDs). For example, for the thermal radiation sources, continuous broadband spectra will result in the restrictions on applications and bring the extra complication into the systems. For the LED sources, the forbidden bands have made it hard to adjust their emission wavelengths. Therefore, the main challenge is to develop novel lighting sources to meet the requirements of NIR applications.

Compared with the existing sources, colloidal QDs NIR LEDs [10–14] has attracted considerable attention due to its unique properties such as narrow full width at half maximum (FWHM), broad absorption, high photoluminescence (PL) quantum yield (QY) and size-tunable emission. Among them, the PbSe bulk material has a small band gap of 0.28 eV at room temperature and a very large exciton Bohr radius of 46 nm. As a result, PbSe QDs show very strong quantum confinement and high QY in NIR region [15–18]. Their band edge PL peaks span over a wide infrared wavelength region of 1–4 μm. The wavelength can be adjusted merely by changing the particle size to cover the particular absorption frequencies of many kinds of gases in the NIR region.

Recently, Choudhury et al. reported solution-processed hybrid NIR LEDs, based on PbSe nanocrystal (NC) lumophores embedded a conjugated polymer forming the nanocomposite active layer [19]. Supran et al. introduced PbS/CdS core-shell QDs and fabricated the related electroluminescent NIR LEDs [20]. Wang et al. fabricated a NIR LED by GaN-based blue LEDs using solid-state PbSe/CdSe/ZnSe core-shell QDs as light conversion materials [21]. Yan et al. employed PbSe QDs as an active layer to convert the excitation source light of GaN LEDs to NIR [22]. However, the PL efficiency of solid-state QDs film was reduced by the non-radiative recombination related to the energy transfer between the QDs with distinct particle sizes [23,24].

In this paper, a liquid-type structure NIR LEDs based on PbSe QDs is developed, where a hydroxy propyl methylcellulose hollow hemisphere is used to protect QDs solution from drying and leaking. Based on the double wavelengths differential detection method, a NIR differential

* Corresponding author.
E-mail address: caofc@sibet.ac.cn (F. Cao).

https://doi.org/10.1016/j.infrared.2019.03.031
Received 3 January 2019; Received in revised form 25 February 2019; Accepted 26 March 2019
Available online 27 March 2019

detection system composed with PbSe QDs NIR LEDs, gas cell with ellipsoid reflector, detector, STM32 main controller and signal processing module is designed to detect C_2H_2 gas. The detection results show that the good concentration measurement is achieved by taking the advantage of the liquid structure PbSe-QDs NIR LEDs. It can be revealed that the liquid-type NIR QDs-LEDs has great potential for gas sensor analysis.

2. Materials and methods

2.1. Fabrication of liquid PbSe QDs NIR LEDs

The liquid-type PbSe QDs NIR LEDs were fabricated by a combination of PbSe QDs solution with blue GaN LEDs. PbSe QDs were synthesized by a modification of a previously reported method [25–27]. The specific fabrication steps were as follows.

Step1: 0.892 g PbO, 5 ml OA and 12 ml ODE were added directly into a three-neck flask, then nitrogen gas flowed into the flask to remove the air thoroughly.
Step2: The three-neck flask was heated to 176 °C until PbO powder completely disappeared and the solution became colorless.
Step3: 6.9 ml Se-TOP solution(containing 0.64 g Se powder) was injected into the solution. 4.64 nm and 6.03 nm QDs particles were obtained by heating the solution at 143 °C for 2 min and 30 s and 7 min, respectively.
Step4: 30 ml of toluene was injected into the three-neck flask and then the flask was submerged in a room-temperature water bath to completely quench the reaction.
Step5: QDs samples were purified by precipitation-redispersion with methanol and hexane. The purified PbSe QDs were redispersed in tetrachloroethylene for spectral characterizations and LED fabrications.
Step6: PbSe QDs solution was filled into a hollow hemisphere via a syringe through a hole, which had the same diameter of 5.6 mm as GaN LEDs and was buckled up easily.
Step7: Sealed with epoxy adhesive, the hemisphere containing QDs solution was placed on a blue GaN chips carefully.

2.2. Characterization of liquid PbSe-QDs NIR LEDs

The absorption spectra was investigated using a UV–visible spectrophotometer (Shimadzu UV-3600). The PL spectra for the as-prepared PbSe QDs solution and liquid-type NIR LEDs were recorded by Omni-λ3007 Spectrograph. The size and shape of PbSe QDs were investigated by transmission electron microscopy (TEM, JEOL FasTEM-2010).

Fig. 1 shows the shape characteristic of PbSe QDs detected by TEM. As seen in Fig. 1, PbSe QDs have spherical structure, uniform particle size and regular distribution. The diameters are 4.64 and 6.03 nm respectively.

The absorption and emission positions of the QDs with diameters of 4.64 nm and 6.03 nm are shown in Fig. 2. Fig. 2(a) shows that the first absorption peak of 4.64 nm PbSe QDs is 1451 nm. The PL peak is 1515 nm with a full width at half-maximum (fwhm) of 165 nm, which covers the entire absorption spectrum of C_2H_2 gas (from 1500 to 1550 nm). Fig. 2(b) shows that the first absorption peak of 6.03 nm PbSe QDs is 1845 nm. The PL peak is 1912 nm with a fwhm of 174 nm.

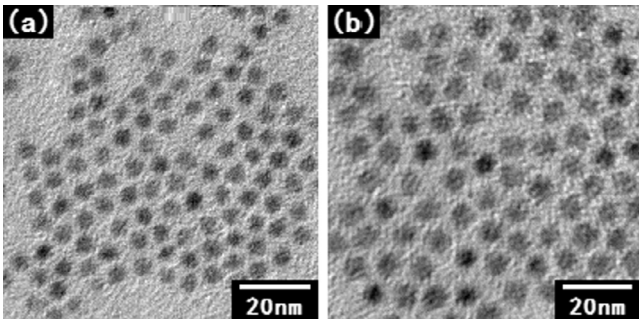

Fig. 1. TEM image of PbSe QDs (a) 4.64 nm (b) 6.1 nm.

The integral sphere spectrum testing system is used to measure the high PL QYs of the encapsulated colloidal solution with the diameters of 4.64 nm and 6.03 nm, which are calculated to be 59% and 31% respectively. A long-term measurement of the high PL QYs lasting for 200 h is carried on. As time goes on, the high PL QYs will decrease gradually. And the high PL QYs will come to 57% and 28%, ordered by the diameter increase.

In order to optimize the NIR LEDs performance, PbSe QDs solutions with five different concentrations for 4.64 and 6.03 nm are separately injected into respective hemispheres. Fig. 3 shows the emission spectra of LEDs depend on the particle sizes and solution concentrations. As seen in Fig. 3, the intensity first increased, and then decreased when the concentration further increased. 4.64 and 6.03 nm PbSe QDs solutions also have optimal concentrations which are 9.3×10^{17} and 4.9×10^{17} QD/ml^{-1} in turn. These features about the intensity depend on concentrations mainly because part of the light emitted by GaN chip will leak through the liquid layer when the concentration is low, while the high concentrations can induce the re-absorption and scattering of light, which will decrease the fluorescence.

The PL spectra of liquid-type NIR LEDs with QDs diameters of 4.64 nm and 6.03 nm under different bias voltages are shown in Fig. 4. It is found that the QDs emission intensity increases significantly along with the bias voltage, suggesting that the higher bias enhances the producing of photons in PbSe QDs. However, the peak positions of two liquid PbSe-QDs NIR LEDs will shift when the voltage increases from 2.7 V to 3.2 V. For example, the red shifts of 2 nm from 1533 to 1535 nm for the LEDs based on 4.6 nm QDs are detected, while the blue shift of 9 nm from 1912 to 1903 nm for the LEDs based on 6.0 nm QDs is measured. The FWHM of emission spectra changes from 165 to 171 nm for 4.64 nm QDs and 174 to 183 nm for 6.03 nm QDs.

The main reason for this phenomenon is that the temperature variation. With the increase of voltage, the temperature of the LEDs will increase persistently. According to the previous report [22], device temperature increasing will induce the shifts of emission spectra, which depends on the size of QDs. Temperature-dependent fluorescence properties of QDs, such as PbSe QDs, have been investigated. With the increasing particle sizes of PbSe QDs, the initially positive temperature coefficient of peak energy becomes zero, and then negative. This property is mainly derived from five factors including band gap of bulk PbSe E_{gap}^{0} (represents kinetic energy only), quantum confinement energy E^{conf}, electron-hole Coulomb attraction energy E_{e-h}, local polarization energy E^{pol} and exciton-phonon coupling E_{e-ph}.

When temperature increases, the leading element is the lattice expansion which will lead to the increase of E_{gap}^{0} for big size PbSe QDs. With the particle size decreases, the temperature-induced variation rate of E^{conf} becomes more influential which would compensate the variation rates of E_{e-ph} and E_{gap}^{0}. Eventually, the temperature coefficient of PbSe QDs reduces to zero at a certain critical particle size and the band gap of PbSe QDs becomes independent on temperature. When the size decreases further, the quantum confinement-induced sized effect increases dramatically and becomes the dominant contribution. The temperature coefficient becomes negative at this moment. This size-dependent temperature coefficient caused the variation of energy gap in the PbSe QDs, thus affected the emission peak positions.

In order to figure out the durability of the liquid-type NIR QD-LEDs, the device is kept working under the bias voltage of 3.0 V continuously. Its PL intensity and radiation power is recorded every 10 h for 30 h. As time goes on, the emission intensity of the LED decreases gradually (Fig. 5(a)) and the radiation power descended slightly (Fig. 5(b)). However, the intensity is still remained at about 90% of original

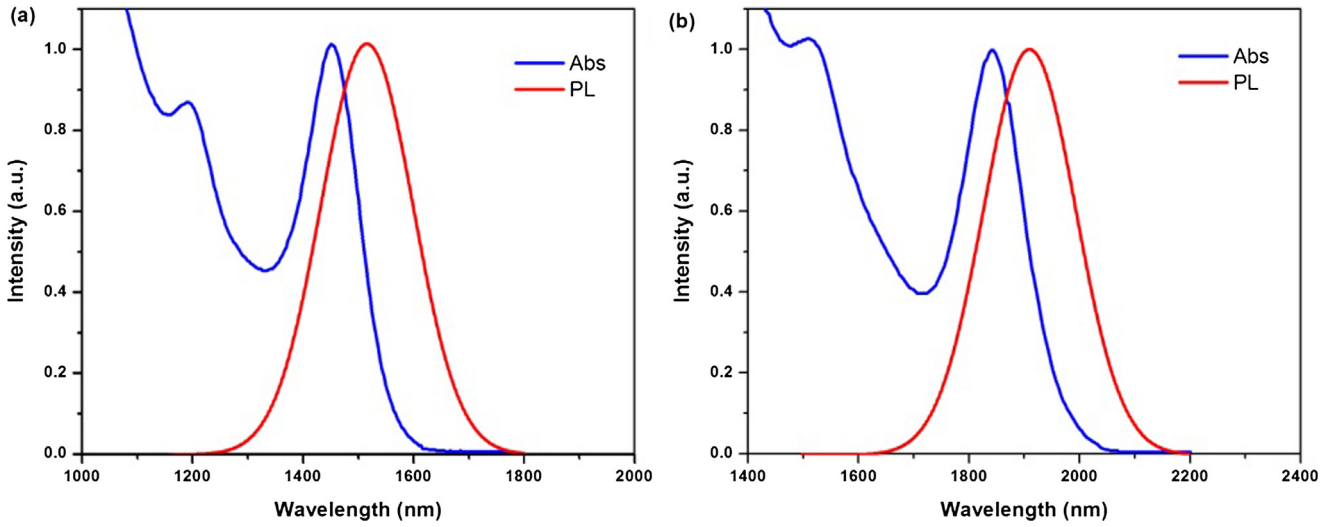

Fig. 2. The PL and absorption spectra of PbSe QDs (a) 4.64 nm (b) 6.03 nm.

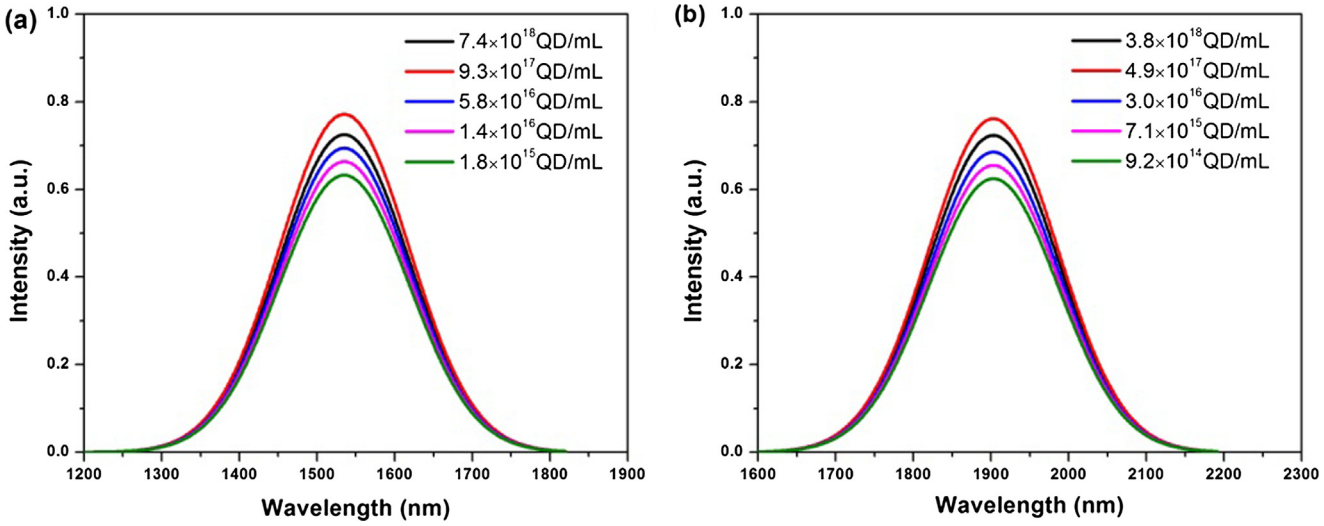

Fig. 3. The PL spectra of liquid-type NIR QD-LEDs with different concentrations for two QDs sizes,(a) 4.64 nm, (b) 6.03 nm, under a bias voltage of 3.0 V.

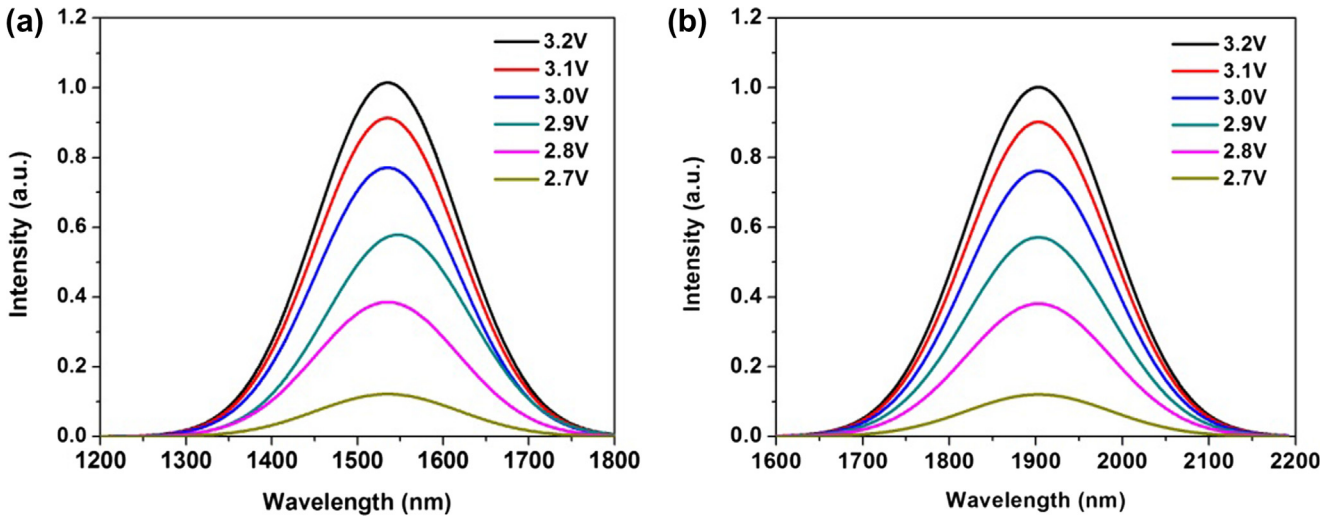

Fig. 4. The PL spectra of liquid-type PbSe QDs NIR LEDs with two sizes under different bias voltages. (a) 4.64 nm (b) 6.03 nm.

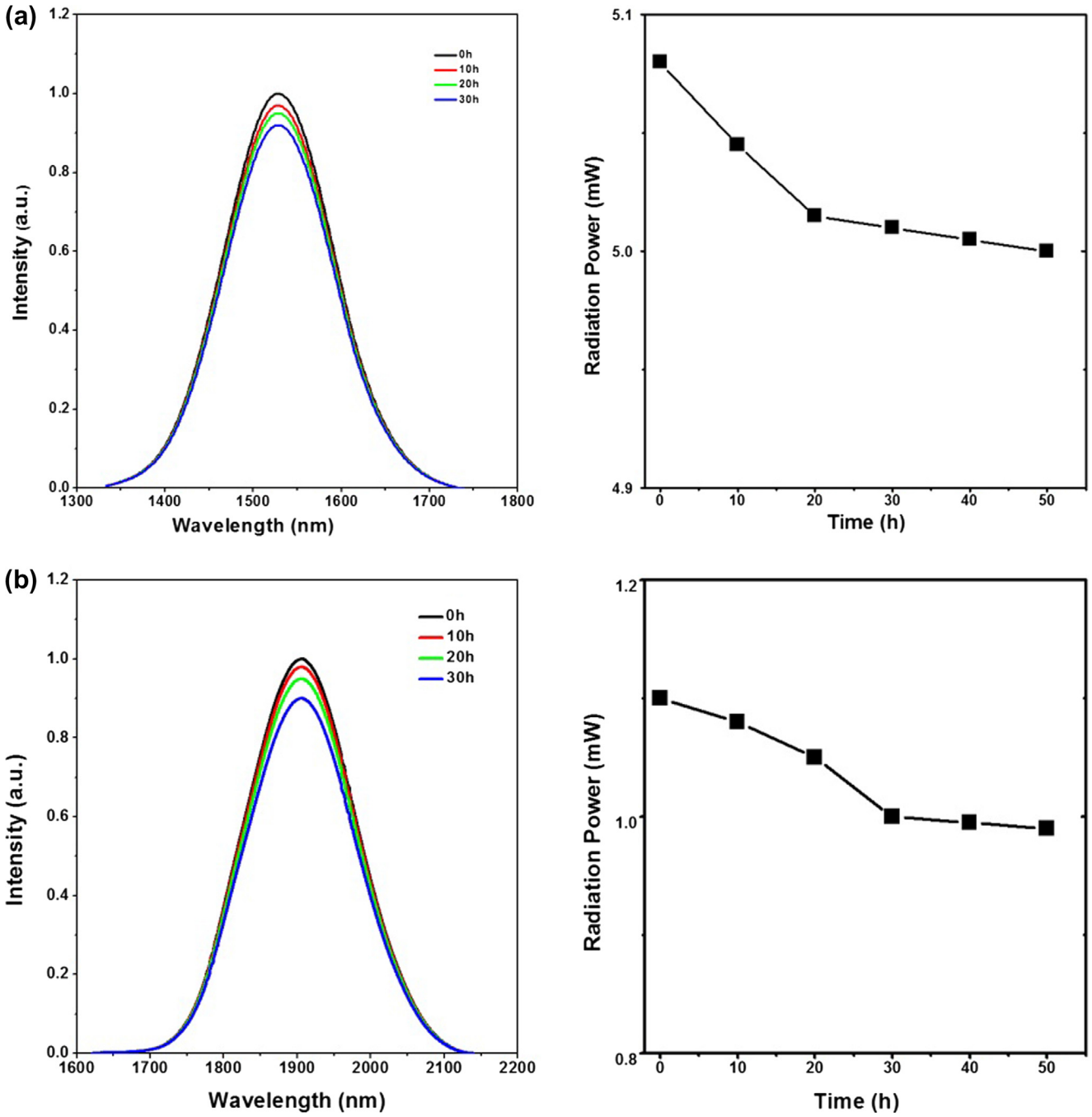

Fig. 5. The spectral stability and radiation power of LEDs with diameters of (a) 4.64 nm (b) 6.03 nm.

intensity after the 30 h continuous work. And the radiation power will come to be 5mW and 1mW for the emission of 4.64 nm and 6.03 nm PbSe QDs under the bias voltage of 3.0 V. In addition, the device is kept working under the bias voltage of 3.0 V continuously to test the lifetime of the LED. It can be found that the half-time of the liquid-type NIR QD-LEDs is about 200 h.

3. Gas detection system

3.1. Selection of gas absorption line

Acetylene has absorption bands in the 730, 1300, 3300 and 6500 cm^{-1} spectral regions. Absorption measurements reported so far have been in the 730, 1300, 3300 and 6500 cm^{-1} bands. In comparison, it is found that the 730, 1300 and 3300 cm^{-1} bands offer stronger vibrational transitions. However, the absorption peaks in 730, 1300 and 3300 cm^{-1} bands overlap with other molecules'. Hence, the wavelength range from 1500 to 1550 nm in near-infrared band becomes the first choice for C_2H_2 detection. According to HITRAN2012 atmospheric molecular spectroscopy database [28], the data of C_2H_2 molecules absorption intensity in the 6500 cm^{-1} band (the wavelength from 1500 nm to 1550 nm) are shown in Fig. 6.

The typical absorption line intensity of atmospheric gases involving H_2O, CO, CH_4 and CO_2 (296 K, 1 atm) are showed in Fig. 7. Fig. 7 shows that the target molecule of C_2H_2 has much stronger absorption than other molecules such as CO, CO_2 and CH_4 in this region. Although the absorption strength of H_2O is stronger than C_2H_2, it is not overlapping with C_2H_2. So the interferences of H_2O, CO, CO_2 and CH_4 can be considered very small.

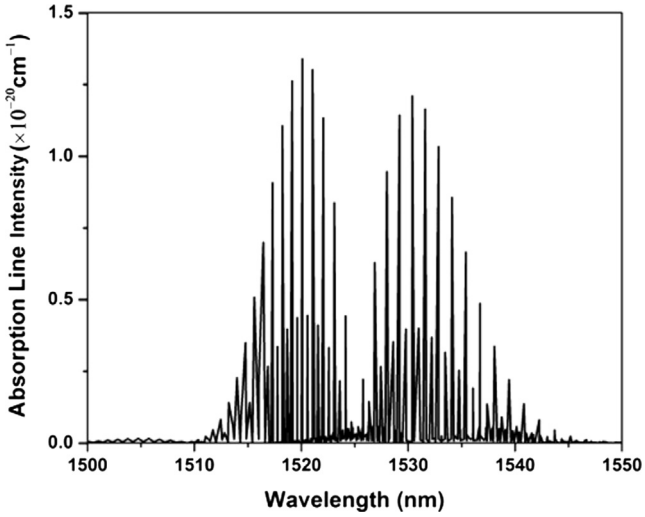

Fig. 6. The absorption line intensity of C_2H_2 in the 6500 cm^{-1} band.

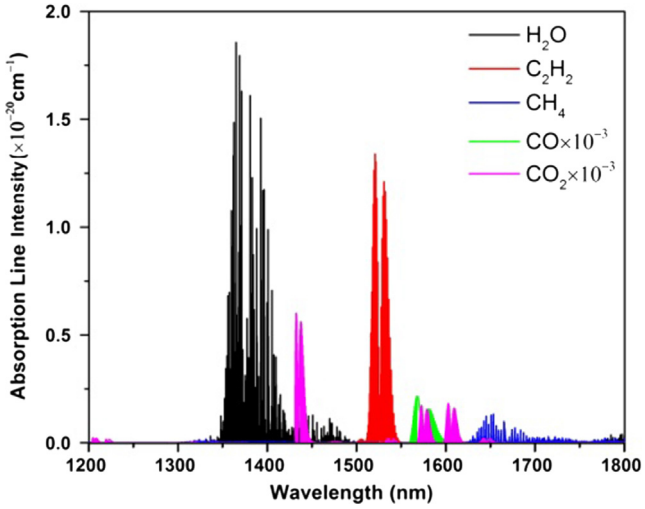

Fig. 7. The Absorption line intensity of C_2H_2, CH_4, CO, CO_2, H_2O from 1200 to 1800 nm.

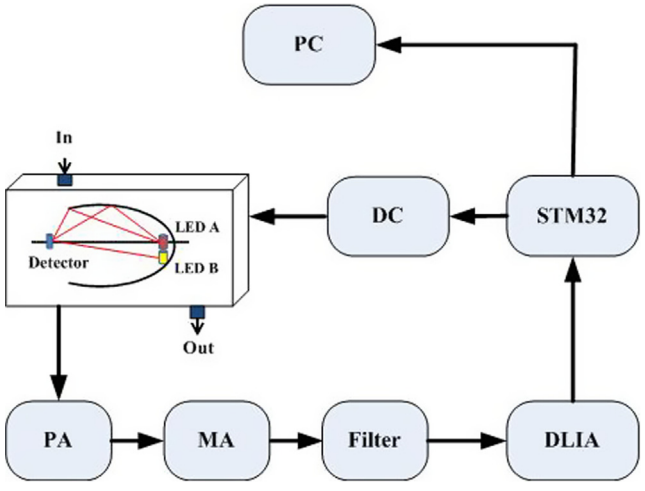

Fig. 8. Structure of the C_2H_2 gas detection system.

3.2. The structure and theory of the system

Fig. 8 shows the structure of C_2H_2 gas detection system based on dual-wavelength differential detection technology. The system consists of PbSe QDs NIR LEDs, gas cell with ellipsoid reflector, PbS photoelectric detector, STM32 main controller and signal processing module. In the system, signal light source LEDA (4.64 nm PbSe-QDs NIR LED) and reference light source LEDB (6.03 nm PbSe-QDs NIR LED) are modulated by the light source driving circuit. Propagating through the gas cell with the ellipsoid reflector, the modulated beam is sensored by the filter-free PbS infrared photoelectric detector in a time-sharing manner. Through pre-amplification, main amplification, filter, digital lock-in amplification, A/D conversion, the detection information is finally displayed on the PC.

According to Lambert-Beer law [29,30], when a light beam passes through the gas, the gas molecules absorb light energy is $I(\lambda)$

$$I(\lambda) = I_0(\lambda)e^{-K(\lambda)CL} \tag{1}$$

where I_0 and I denote the input and output light intensities respectively; K is the absorption coefficient of C_2H_2 gas; C is the C_2H_2 gas concentration; and L is the length of absorption path.

Define the signal wavelength is λ_1, the reference wavelength is λ_2; the response of the detector at λ_1 and λ_2 is $R(\lambda_1)$ and $R(\lambda_2)$; the background noise of the detector at λ_1 and λ_2 is $n_0(\lambda_1)$ and $n_0(\lambda_2)$. The output voltage of the signal channel is $V(\lambda_1)$

$$V(\lambda_1) = R(\lambda_1)I_0(\lambda_1)e^{-K(\lambda_1)CL} + n_0(\lambda_1) \tag{2}$$

The output voltage of the reference channel is $V(\lambda_2)$

$$V(\lambda_2) = R(\lambda_2)I_0(\lambda_2)e^{-K(\lambda_2)CL} + n_0(\lambda_2) \tag{3}$$

Assume $\Delta V = V(\lambda_1) - V(\lambda_2)$, the differential ratio of the output signal $m$can be wtitten:

$$\begin{aligned} m &= \frac{\Delta V}{V(\lambda_2)} = \frac{R(\lambda_1)I_0(\lambda_1)e^{-K(\lambda_1)CL} - R(\lambda_2)I_0(\lambda_2)e^{-K(\lambda_2)CL}}{R(\lambda_2)I_0(\lambda_2)e^{-K(\lambda_2)CL}} + \frac{n_0(\lambda_1) - n_0(\lambda_2)}{R(\lambda_2)I_0(\lambda_2)e^{-K(\lambda_2)CL}} \\ &\approx \frac{R(\lambda_1)I_0(\lambda_1)e^{-K(\lambda_1)CL} - R(\lambda_2)I_0(\lambda_2)e^{-K(\lambda_2)CL}}{R(\lambda_2)I_0(\lambda_2)e^{-K(\lambda_2)CL}} = \frac{R(\lambda_1)I_0(\lambda_1)}{R(\lambda_2)I_0(\lambda_2)}\left(e^{-[K(\lambda_1)-K(\lambda_2)]CL} - 1\right) \end{aligned} \tag{4}$$

The gas concentration C can be expressed as

$$C = \frac{1}{[K(\lambda_2) - K(\lambda_1)]L} \ln\left[\left(1 + \frac{\Delta V}{V(\lambda_2)}\right)\frac{R(\lambda_2)I_0(\lambda_2)}{R(\lambda_1)I_0(\lambda_1)}\right] \tag{5}$$

3.3. The design of the gas cell

According to Lambert's law, the larger the light path of the gas cell, the more obvious the gas absorption is. In this paper, the gas cell with ellpsoid reflector is designed to increase the absorption path. The structure of the gas cell is shown in Fig. 9.

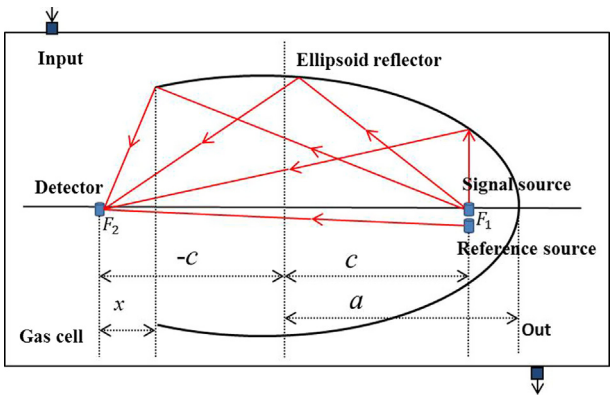

Fig. 9. Diagram of ellipsoid reflctor gas cell.

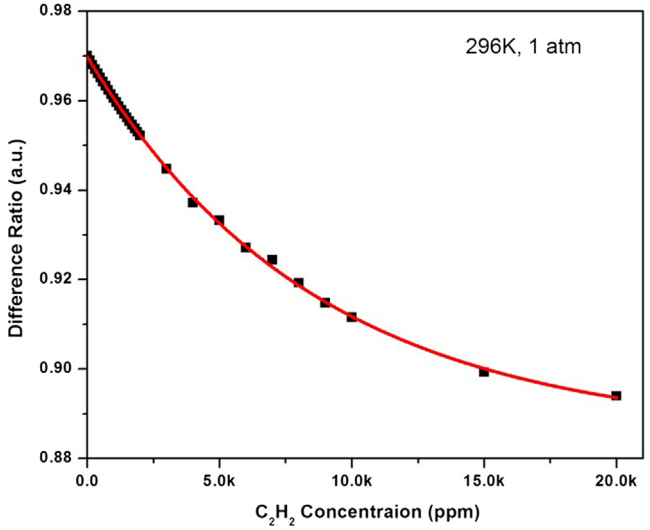

Fig. 10. The amplitude of signal difference ratio fitted curve under different C_2H_2 concentration.

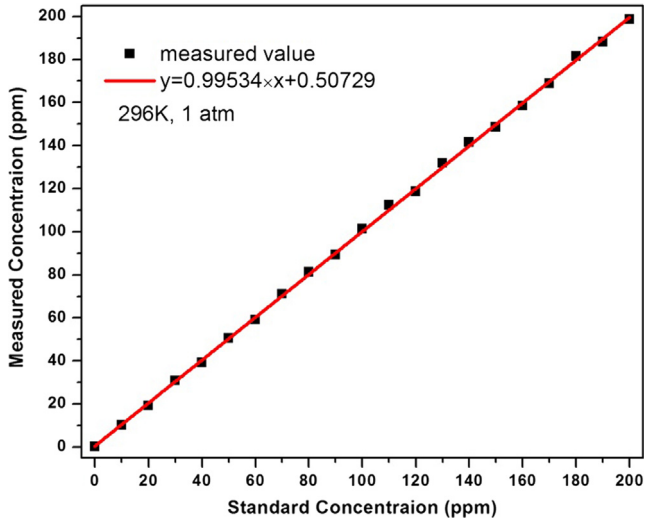

Fig. 11. The comparison between standard and measured concentration of C_2H_2.

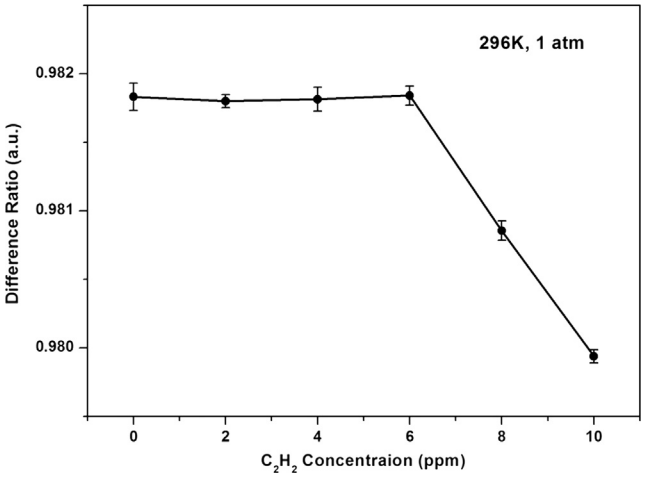

Fig. 13. The difference ratio curve under low concentration (0–10 ppm).

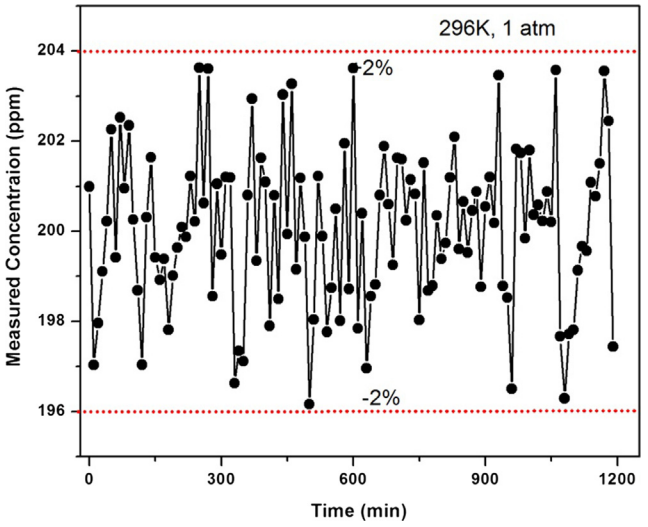

Fig. 14. Experiment on system stability.

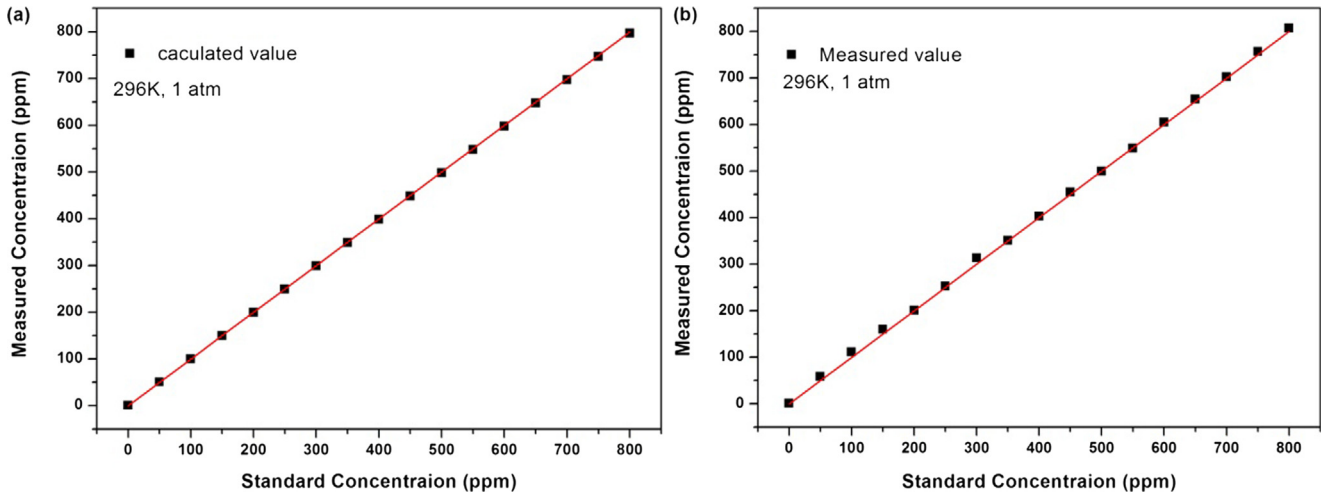

Fig. 12. The accuracy curves of C_2H_2 (a) calculated by the curve fitting formula and (b) measured actually after 1000 ppm H_2O was loaded into the gas cell.

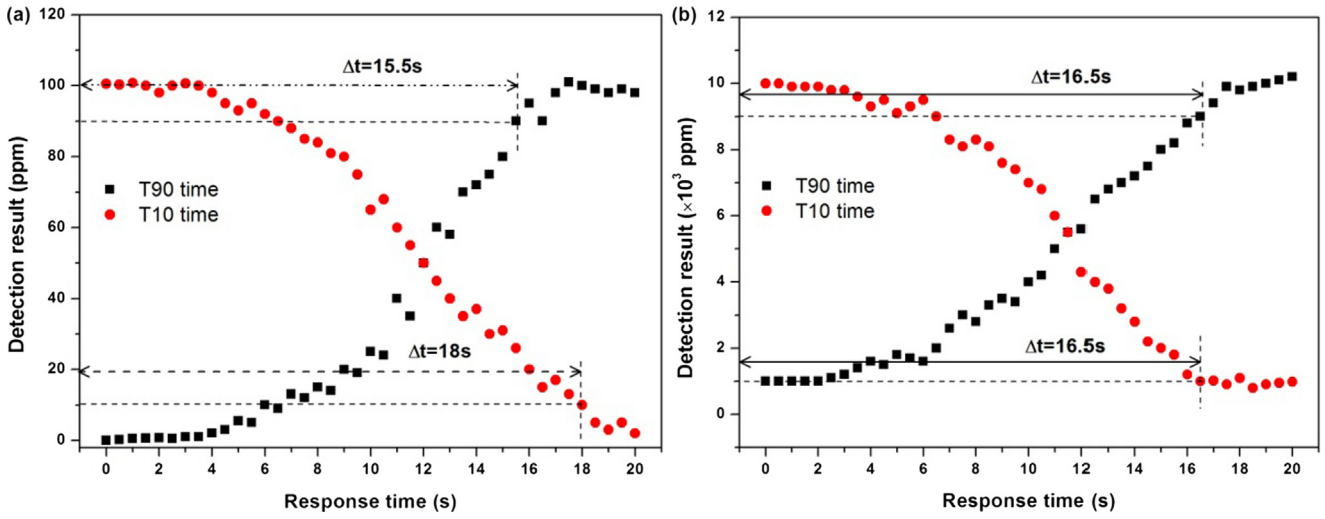

Fig. 15. Experimental results of response time in (a) low concentration and (b) high concentration range.

As shown in Fig. 8, a and c are the semimajor axis and the focal length of the ellipsoid reflector respectively. x is the open length of ellipsoid reflector. The focal point coordinates are $F_1(+c, 0)$ and $F_2(-c, 0)$. The signal light source LEDA is placed at F_1; the reference light source LEDB is placed at a defocus position, and the detector is on F_2. The related parameters are set as follows: $a = 4.18cm$, $c = 3.98cm$, $x = 0.36cm$. It can be proved that the structure can enhance the intensity of the output signal, which can be used to improve the detection sensitivity and precision in gas detection system.

4. Experiment and analysis

4.1. The concentration detection results

By using the designed system, the concentrations of C_2H_2 within 0–20000 ppm are measured (296 K, 1 atm). Fig. 10 shows the difference ratio of the output signal fitting curve under 31 standard concentrations of C_2H_2.

The curve fitting is made using Matlab, and the fitting formula can be obtained as

$$m = 0.06624 \times e^{-0.00012C} + 0.91375 \quad (6)$$

where, m represents the measured differential ratio; and C is the concentration of C_2H_2 gas. The relationship between m and C satisfies the Lambert's law.

4.2. The precision of the system

In addition, in order to get the detection limit of the system, 21 standard concentrations of C_2H_2 gas within 0–800 ppm are measured by the system. Fig. 11 shows the comparison between the measured gas concentration and the standard gas concentration. The curve fitting is made, and the fitting formula is

$$y = 0.99534 \times x + 0.50729 \quad (7)$$

Fig. 11 indicates that the maximum relative detection error of the system is less than ± 3% within 0–200 ppm.

Air is a mixture of many gases mainly including N_2, CO_2, and H_2O. It is necessary to eliminate their impacts to the measurement result. N_2 has no absorption in the emission spectrum area of this NIR LED. The absorption of CO_2 in this area is very weak. However, there is still some overlap between H_2O absorption spectrum and the emission spectrum of the NIR LED. Therefore, we load the mixed gases including a certain amount of C_2H_2 (0–800 ppm) and 1000 ppm H_2O into the detection system. The concentrations of C_2H_2 are calculated by the above curve fitting formula which are compared with the standard concentration shown in Fig. 12.

Fig. 12 exhibits the comparison between calculated by the curve fitting formula and measured actually after 1000 ppm H_2O was loaded into the gas cell. Owning to the absorption of H_2O, the measured concentrations of C_2H_2 are a little higher than the standard concentration. However, the impact is small. The light sources based on PbSe quantum dots have plenty advantages such as small size, high efficiency, high modulation rate and low price. However, there is still limitation about this kind of light sources in the field of gas detection. If there is absorption spectra overlap between the detected gas and the interferential gas, it is hard to get the exact concentration of detected gas. The interferential gas would affect the detection result.

When the concentration of C_2H_2 gas ranges from 0 to 10 ppm, the difference ratio curve is shown in Fig. 13. Fig. 13 illustrates that the amplitude of the difference ratio changes obviously when the concentration of C_2H_2 gas reaches 10 ppm. Therefore, the conclusion can be obtained that the detection limit of the system is 10 ppm.

4.3. The stability and response time of the system

In order to test the stability of the detection system, a long-term measurment lasting for 20 h with 200 ppm C_2H_2 gas sample is carried on. The detection results are collected every 10 min. The 120 sets of acquisition data are shown in Fig. 14. As seen in Fig. 14, the output measurement concentration range of the system is 196–204 ppm, and the maximum relative detection error is less than ± 2%. It can be concluded that the system is stable and reliable.

The response time test of the sensor system in low concentration (0–100 ppm) and high concentration (1000–10000 ppm) range is carried out. C_2H_2 gas is loaded into the designed system. The concentration measurement results of the system are stored in real time by STM32. After the reading of the system is basically stable, pure N_2 is loaded into the gas cell to reduce its internal concentration to about 0. Experimental results of response time in low concentration range are shown in Fig. 15.

According to the previous report [31], the T_{90} (time to achieve 90% actually concentration) and T_{10} (time to achieve 10% actually concentration) of response time of the sensor system is related to the structural parameters of the chamber. As seen in Fig. 15, when the concentration of the C_2H_2 gas varies from 0 to 100 ppm, the T_{90} and T_{10} time are 15.5 s and 18 s, respectively. When the concentration of the C_2H_2 gas varies from 1000 to 10000 ppm, the T_{90} and T_{10} time are about 16.5 s.

5. Conclusion

In summary, a new and facile liquid-type NIR LEDs utilizing PbSe QDs solution as a downconversion layer is reported. Employing the NIR PbSe-QDs LEDs, a near-infrared C_2H_2 gas differential detection system based on the NIR absorption spectroscopy technique is developed. The detection results show that the good accuracy, stability and reliablity are achieved by taking the advantage of the liquid structure PbSe QDs NIR LEDs, in which the loss related to the energy transfer is remarkably lower than that in the solidstate film. The NIR QD-based LEDs exhibits the highest value among the previous reports of NIR QD-based LEDs and is comparable to the commercial NIR LEDs. Therefore, the as-fabricated liquid-type NIR QD-LEDs has great potential for gas sensing detection.

Conflict of Interest

The authors have declared that no conflict of interest exists.

Acknowledgments

This work is supported by the Natural Science Foundation of China, China (61805021, 61722504, 61675086), Key Technology Research and Development Projects of Jilin Province, China (20180201063YY), Science and Technology Plan Project of Jilin Province, China (2016LY402L01), Natural Science Foundation of Jilin Province, China (20170101049JC), and Department of Science and Technology Plan Projects of Jilin Province, China (JJKH20191196KJ).

References

[1] P.F. Cheng, Y.H. Hu, Acetylene adsorption on defected MIL-53, Int. J. Energy Res. 40 (2016) 846–852.
[2] K. Chen, Z. Gong, Q. Yu, Fiber-amplifier-enhanced resonant photoacoustic sensor for sub-ppb level acetylene detection, Sens. Actuat. A: Phys. 274 (2018) 184–188.
[3] K.C. Utsav, F.N. Ehson, F. Aamir, A mid-infrared absorption diagnostic for acetylene detection, Appl. Phys. B: Lasers Opt. 120 (2015) 223–232.
[4] A.L. Sahlberg, J. Kiefer, M. Aldén, Z. Li, Mid-infrared pumped laser-induced thermal grating spectroscopy for detection of acetylene in the visible spectral range, Appl. Spectrosc. 70 (2016) 1034–1043.
[5] Y.F. Ma, Y. He, L.G. Zhang, Ultra-high sensitive acetylene detection using quartz-enhanced photoacoustic spectroscopy with a fiber amplified diode laser and a 30.72 kHz quartz tuning fork, Appl. Phys. Lett. 110 (2017) 1–5.
[6] X.X. Xing, H.W. Qin, W.W. Shang, Research of spectrum matching method for PbSe quantum dots luminescence spectrum and gas absorption spectrum, Sepctrpsc. Spect. Analy. 36 (2016) 3588–3591 (in Chinese).
[7] Q.X. He, H.F. Liu, B. Li, J.Q. Pan, L.J. Wang, C.T. Zheng, Y.D. Wang, Online detection system on acetylene with tunable diode laser absorption spectroscopy method, Sepctrpsc. Spect. Anal. 36 (2016) 3501–3505 (in Chinese).
[8] Q.X. He, C.T. Zheng, H.F. Liu, B. Li, Y.D. Wang, F.K. Tittel, A near-infrared acetylene detection system based on a 1.534μm tunable diode laser and a miniature gas chamber, Infrared Phys. Technol. 75 (2016) 93–99.
[9] M. Dong, C.T. Zheng, D. Yao, G. Zhong, S. Miao, W. Ye, Y.D. Wang, F.K. Tittel, Double-range near-infrared acetylene detection using a dual spot-ring Herriott cell (DSR-HC), Opt. Exp. 26 (2018) 12081–12091.
[10] X.Y. Zhang, C. Sun, Y. Zhang, H. Wu, C. Ji, Y. Chuai, P. Wang, S. Wen, C. Zhang, W.W. Yu, Bright perovskite nanocrystal films for efficient light-emitting devices, J. Phys. Chem. Lett. 7 (2016) 4602–4610.
[11] Y. Zhang, Q.Q. Dai, X.B. Li, B. Zou, Y.D. Wang, W.W. Yu, Beneficial effect of tributylphosphine to the photoluminescence of PbSe and PbSe/CdSe nanocrystals, J. Nanopart. Res. 13 (2011) 3721–3729.
[12] W.J. Hu, R. Henderson, Y. Zhang, G. You, L. Wei, Y. Bai, J. Wang, J. Xu, Near-infrared quantum dot light emitting diodes employing electron transport nanocrystals in a layered architecture, Nanotechnology 23 (2012) 375202–375208.
[13] P.F. Gu, Y. Zhang, Y. Feng, T.Q. Zhang, H. Chu, T. Cui, Y. Wang, J. Zhao, W.W. Yu, Real-time and on-chip surface temperature sensing of GaN LED chips using PbSe quantum dots, Nanoscale 5 (2013) 10481–10486.
[14] C.Y. Ji, Y. Zhang, T.Q. Zhang, W.Y. Liu, X.Y. Zhang, H.Z. Shen, Y. Wang, W.Z. Gao, Y.D. Wang, J. Zhao, W.W. Yu, Temperature-dependent photoluminescence of Ag_2Se quantum dots, J. Phys. Chem. C 119 (2015) 13841–13846.
[15] J. Chen, Y. Li, L. Wang, T. Zhou, R.J. Xie, Achieving deep-red-to-near-infrared emissions in Sn-doped Cu-In-S/ZnS quantum dots for red-enhanced white LEDs and near-infrared LEDs, Nanoscale 10 (2018) 9788–9795.
[16] W. Qiu, Z. Xiao, K. Roh, N.K. Noel, A. Shapiro, P. Heremans, B.P. Rand, Mixed lead-tin halide perovskites for efficient and wavelength-tunable near-infrared light-emitting diodes, Adv. Mater. (2018) e1806105.
[17] R.S. Sanchez, E. Binetti, J.A. Torre, G. Garcia-Belmonte, M. Striccoli, I. Mora-Sero, All solution processed low turn-on voltage near infrared LEDs based on core-shell PbS-CdS quantum dots with inverted device structure, Nanoscale 6 (2014) 8551–8556.
[18] X.W. Gong, Z.Y. Yang, G. Walters, R. Comin, Z.J. Ning, E. Beauregard, V. Adinolfi, O. Voznyy, E.H. Sargent, Highly efficient quantum dot near-infrared light-emitting diodes, Nature 10 (2016) 253–260.
[19] K.R. Choudhury, D.W. Song, F. So, Efficient solution-processed hybrid polymer-nanocrystal near infrared light-emitting devices, Org. Electron. 11 (2010) 23–28.
[20] G.J. Supran, K.W. Song, G.W. Hwang, R.E. Correa, J. Scherer, E.A. Dauler, Y. Shirasaki, M.G. Bawendi, V. Bulović, High performance shortwave infrared light emitting devices using core-shell (PbS-CdS) colloidal quantum dots, Adv. Mater. 27 (2015) 1437–1442.
[21] T.Y. Wang, P. Wang, H.L. Wang, T.Q. Zhang, Solar cells of the inorganic materials based on PbSe/CdSe core/shell nanocrystals, Appl. Mechan. Mater. 737 (2015) 119–122.
[22] L. Yan, X.Y. Shen, Y. Zhang, X.Y. Zhang, Y. Feng, J.Z. Yin, J. Zhao, W.W. Yu, Near-infrared light emitting diodes using PbSe quantum dots, RSC Adv. 5 (2015) 54109–54123.
[23] C. Javaux, B. Mahler, B. Dubertret, A. Shabaev, A.V. Rodina, A.L. Efros, D.R. Yakovlev, F. Liu, M. Bayer, G. Camps, L. Biadala, S. Buil, X. Quelin, J.P. Hermier, Thermal activation of non-radiative Auger recombination in charged colloidal nanocrystals, Nat. Nanotechnol. 8 (2013) 206–218.
[24] Y.S. Park, W.K. Bae, L.A. Padilha, J.M. Pietryga, V.I. Klimov, Effect of the core/shell interface on auger recombination evaluated by single-quantum-dot spectroscopy, Nano Lett. 14 (2014) 396–402.
[25] W.J. Hu, R. Henderson, Y. Zhang, G. You, L. Wei, Y. Bai, J. Wang, J. Xu, Near-infrared quantum dot light emitting diodes employing electron transport nanocrystals in a layered architecture, Nanotechnology 23 (2012) 375202.
[26] X.X. Xing, Y.M. Lei, L.M. Du, W.W. Shang, P. Guo, Theoretical research on ellipsoidal structure methane gas detection based on near infrared light sources of PbSe Quantum dots, Nanomaterials (2017) 6548380.
[27] L. Yan, Y. Zhang, T.Q. Zhang, Y. Feng, K.B. Zhu, D. Wang, T. Cui, J.Z. Yin, Y.D. Wang, J. Zhao, W.W. Yu, Tunable near-infrared luminescence of PbSe quantum dots for multigas analysis, Anal. Chem. 86 (2014) 11312–11320.
[28] L.S. Rothman, I.E. Gordon, Y. Babikov, A. Barbe, D.C. Benner, P.F. Bernath, M. Birk, L. Bizzocchi, V. Boudon, L.R. Brown, A. Campargue, K. Chance, E.A. Cohen, L.H. Coudert, V.M. Devi, B.J. Drouin, A. Fayt, J.M. Flaud, R.R. Gamache, J.J. Harrison, J.M. Hartmann, C. Hill, J.T. Hodges, D. Jacquemart, A. Jolly, J. Lamouroux, The HITRAN2012 molecular spectroscopic database, J. Quant. Spectrosc. Radiat. Transf. 130 (2013) 4–50.
[29] F. Scholkmann, S. Kleiser, A.J. Metz, R. Zimmermann, J.M. Pavia, M. Wolf, A review on continuous wave functional near-infrared spectroscopy and imaging instrumentation and methodology, NeuroImage 85 (2014) 6–27.
[30] J.H. Yang, N.J. Kramer, K.S. Schramke, L.M. Wheeler, L.V. Besteiro, C.J. HoganJr, A.O. Govorov, U.R. Kortshagen, Broadband absorbing exciton-plasmon metafluids with narrow transparency windows, Nano Lett. 16 (2016) 1472–1477.
[31] W.L. Ye, C.T. Zheng, Y.D. Wang, Modeling and experimental study on response time of a mid-infrared CH_4 detection device, J. Opt. Laser (2015) 1030–1035.